

# Key Role of Choline Head Groups in Large Unilamellar Phospholipid Vesicles for the Interaction with and Rupture by Silica Nanoparticles

Regina Leibe, Susanne Fritsch-Decker, Florian Gussmann, Ane Marit Wagbo, Parvesh Wadhvani, Silvia Diabaté, Wolfgang Wenzel, Anne S. Ulrich, and Carsten Weiss\*

For highly abundant silica nanomaterials, detrimental effects on proteins and phospholipids are postulated as critical molecular initiating events that involve hydrogen-bonding, hydrophobic, and/or hydrophilic interactions. Here, large unilamellar vesicles with various well-defined phospholipid compositions are used as biomimetic models to recapitulate membranolysis, a process known to be induced by silica nanoparticles in human cells. Differential analysis of the dominant phospholipids determined in membranes of alveolar lung epithelial cells demonstrates that the quaternary ammonium head groups of phosphatidylcholine and sphingomyelin play a critical and dose-dependent role in vesicle binding and rupture by amorphous colloidal silica nanoparticles. Surface modification by either protein adsorption or by covalent coupling of carboxyl groups suppresses the disintegration of these lipid vesicles, as well as membranolysis in human A549 lung epithelial cells by the silica nanoparticles. Furthermore, molecular modeling suggests a preferential affinity of silanol groups for choline head groups, which is also modulated by the pH value. Biomimetic lipid vesicles can thus be used to better understand specific phospholipid–nanoparticle interactions at the molecular level to support the rational design of safe advanced materials.

synthetic amorphous silica nanoparticles (SiO<sub>2</sub>-NPs) with special and promising surface properties.<sup>[4]</sup> SiO<sub>2</sub>-NPs are particularly interesting for the emerging field of nanomedicine as versatile theranostic agents.<sup>[5–7]</sup> However, adverse effects must be avoided to fully exploit the potential of nanobiomaterials. Several adverse outcome pathways for nanomaterials have been identified thus far.<sup>[8–10]</sup> Specifically, the interaction with the silica surface can trigger denaturation of proteins,<sup>[11]</sup> which bind to dedicated receptors involved in inflammation,<sup>[12]</sup> or perturbs the integrity of cellular membranes as manifested, e.g., in hemolysis.<sup>[13,14]</sup> Although the rupture of the lysosomal or plasma membranes is a critical aspect of SiO<sub>2</sub>-NP toxicity, the underlying mechanism is poorly understood. Potential membrane damage has been attributed to the production of reactive oxygen species resulting from homolytic cleavage of strained three-membered siloxane rings in the case of fumed SiO<sub>2</sub>-NPs.<sup>[15]</sup> Alternatively, direct molecular interaction of the silica surface with proteins and phospholipids might be essential for membranolysis. Indeed, the degree of cytotoxicity and hemolysis correlates with the available external silica surface area.<sup>[16,17]</sup> Coating the silica surface by, e.g., protein adsorption has been shown to suppress the lysis of epithelial and red blood

## 1. Introduction

A fundamental understanding of the mechanisms of nanomaterial interaction with living systems is key for the safe implementation and development of advanced materials.<sup>[1–3]</sup> The most abundant class of nanomaterials is represented by

NPs.<sup>[15]</sup> Alternatively, direct molecular interaction of the silica surface with proteins and phospholipids might be essential for membranolysis. Indeed, the degree of cytotoxicity and hemolysis correlates with the available external silica surface area.<sup>[16,17]</sup> Coating the silica surface by, e.g., protein adsorption has been shown to suppress the lysis of epithelial and red blood

R. Leibe, S. Fritsch-Decker, A. M. Wagbo, S. Diabaté, C. Weiss  
Institute of Biological and Chemical Systems – Biological Information  
Processing (IBCS-BIP)  
Karlsruhe Institute of Technology (KIT)  
Hermann-von-Helmholtz-Platz 1, D-76344 Eggenstein-Leopoldshafen,  
Germany  
E-mail: carsten.weiss@kit.edu

F. Gussmann, W. Wenzel  
Institute of Nanotechnology (INT)  
KIT  
Hermann-von-Helmholtz-Platz 1, D-76344 Eggenstein-Leopoldshafen,  
Germany  
P. Wadhvani, A. S. Ulrich  
Institute of Biological Interfaces (IBG-2)  
KIT  
Hermann-von-Helmholtz-Platz 1, D-76344 Eggenstein-Leopoldshafen,  
Germany

 The ORCID identification number(s) for the author(s) of this article can be found under <https://doi.org/10.1002/smll.202207593>.

© 2023 The Authors. Small published by Wiley-VCH GmbH. This is an open access article under the terms of the Creative Commons Attribution-NonCommercial License, which permits use, distribution and reproduction in any medium, provided the original work is properly cited and is not used for commercial purposes.

DOI: 10.1002/smll.202207593

cells.<sup>[18–20]</sup> Several types of binding forces have been postulated, including: 1) ionic interactions of negatively charged silanol groups with positively charged amino groups or quaternary ammonium ions; 2) hydrogen bonding with electron donor atoms such as nitrogen or oxygen; 3) hydrophobic bonding between the siloxane surface and biopolymers; and 4) van der Waals forces.<sup>[21–24]</sup> As SiO<sub>2</sub>-NPs increase the permeability of lipid bilayers, phospholipids, in addition to proteins, are direct targets.<sup>[25]</sup> Anionic NPs, including silica, also induce local gel formation in liposomes, resulting in less fluidic membranes at the site of interaction.<sup>[26]</sup>

In the past, various membrane models have been employed to study the interaction of silica NPs with phospholipids.<sup>[27]</sup> These models include lipid monolayers, supported lipid bilayers (SLBs) and lipid vesicles. In lipid monolayers, only one layer can be studied and lipids are not completely submerged in the water phase, potentially affecting the NP–phospholipid interaction. In the case of SLBs, a lipid bilayer interaction with NPs can be quantitatively monitored. However, in both cases only a planar surface is presented to the NPs neglecting the curvature of biological membranes. Therefore, most often, lipid vesicles are studied, which are submerged in an aqueous phase and where lipids are laterally more mobile. There are different sizes of lipid vesicles available, starting from small unilamellar vesicles (SUVs) of about 20–100 nm, followed by large unilamellar vesicles (LUVs) in the range of 100–1000 nm, up to giant unilamellar vesicles (GUVs) covering a size range of 1–200 μm.<sup>[28]</sup> Although GUVs are approaching the size of cells, with a curvature more comparable to the cell membrane, the stability of SUVs and LUVs is much higher and allows for proper stirring and mixing with NPs. Binding of silica NPs has been documented for lipid monolayers<sup>[29]</sup> composed of equal amounts of dioleoyl phosphatidylcholine (DOPC), sphingomyelin (SM), and cholesterol. Similarly, for SLBs composed of palmitoyl-oleoyl phosphatidylcholine (POPC)<sup>[30]</sup> or DOPC,<sup>[31]</sup> binding of silica NPs has been observed, which can be inhibited by addition of serum proteins. In SLBs composed of DOPC, silica NPs increased the membrane permeability evidenced by enhanced electroconductivity.<sup>[25]</sup> Numerous studies have also addressed the interaction of silica NPs with lipid vesicles.<sup>[27]</sup> One of the pioneering work showed binding of colloidal silica NPs to SUVs composed of DOPC and dioleoylphosphatidylserine (ratio 4:1), which leads to rupture in case of positively, neutral, or slightly negatively charged SUVs.<sup>[32]</sup> Investigations by cryo electron microscopy have visualized NP attachment to SUVs and the subsequent formation of an SLB on the NP surface, which coincides with vesicle rupture. Increasing the proportion of phosphatidylserine (PS) versus DOPC (ratio 1:1), rendering the SUVs negatively charged, suppressed binding and rupture by silica NPs, which indicates that electrostatic forces play a critical role in these processes. Later studies explored the impact of the relative size of silica particles and lipid vesicles on the mechanism of membrane rupture, which was measured by the release of a fluorescent dye from the vesicles.<sup>[33]</sup> LUVs (400 nm) made of either DOPC only or a 2:1 mixture of DOPC and palmitoyl-oleoyl-phosphatidylglycerol (POPG) were used for interaction studies with colloidal silica NPs of different sizes (50, 200, and 500 nm). While larger particles led to the formation of an SLB on their surface, the 50 nm NPs

were engulfed into the LUVs and presumably triggered a local depletion of phospholipids, followed by a collapse of the vesicle membrane at high NP concentrations (particle/liposome ratio > 8). The inclusion of negatively charged POPG reduced vesicle rupture, as evidenced by lower dye leakage for both 50 and 200 nm silica particles. Furthermore, surface carboxylation or amination of 50 nm silica NPs largely suppressed dye release by LUVs, suggesting that either critical functional groups at the silica surface, such as silanol groups, were replaced, or the carboxyl or amine groups themselves interfered with the NP/phospholipid interaction. Finally, the coating of 100 nm silica particles with the protein avidin through physisorption also reduced dye leakage from DOPC LUVs. The impact of the relative size of silica particles on vesicle disintegration was studied by employing either fluorescence or electron microscopy to monitor the structure of DOPC GUVs (4–20 μm) or LUVs (300 nm), respectively. For LUVs, particles smaller than 30 nm only adhered to the vesicles, while larger particles (30–200 nm) were engulfed and covered by a lipid bilayer, which resulted in vesicle rupture.<sup>[34]</sup> In the case of GUVs, small 18 nm silica particles bound and decreased the lateral mobility of phospholipids, generating micro-sized holes. However, larger particles (>78 nm) provoked membrane wrapping and collapse of the vesicles.<sup>[35]</sup> Similar findings on vesicle rupture were obtained in another study with GUVs and silica nanoparticles, in which the interaction of silica with the P<sup>-</sup>-N<sup>+</sup> dipole in the phosphocholine head group of DOPC was suggested to induce membrane gelation.<sup>[36]</sup> Indeed, when LUVs consisting of different physiological and artificial phosphatidylcholines were incubated with either carboxyl-modified polystyrene or plain silica NPs, local gelation of the lipid bilayer was observed.<sup>[37]</sup>

Thus far, mostly vesicles (SUVs, LUVs, GUVs) with a fixed DOPC (PC) content were utilized (either 100% PC or a fixed ratio with other lipids) and the relative PC content was not systematically varied. Thus, the concentration-dependent impact of PC on binding and rupture of vesicles by silica NPs remains unexplored. Here, we aimed to investigate whether different thresholds of PC in phospholipid bilayers of LUVs are necessary for binding of and rupture by amorphous silica NPs. As cellular membranes contain a relative high content of PC, as well as a variety of other phospholipids, we first sought to mimic the membrane composition of lung epithelial cells by tailoring the relative phospholipid ratio of LUVs. Since the lung is one of the main target organs upon NP exposure, adverse reactions are frequently assessed in cell culture experiments employing, e.g., A549 lung adenocarcinoma cells. Indeed, toxic effects induced by nanomaterials, such as membrane damage, observed in A549 cells *in vitro* have been shown to correlate well with pulmonary toxicity *in vivo* (i.e., pulmonary exposure conducted in rats).<sup>[38,39]</sup> Instead of simply using LUVs composed solely of PC or other artificial lipid compositions containing PC, we decided to examine the interaction of silica NPs and LUVs with a more physiologically relevant phospholipid composition. To this end, LUVs were generated using the main phospholipids (PC, palmitoyl-oleoyl-phosphatidylethanolamine (PE), SM) in proportions similar to those determined in A549 cell membranes.<sup>[40]</sup> The impact of silica NPs on these LUVs was then compared to the membranolytic effects observed in A549 cells. Following these initial studies, a more reductionist

approach was taken to focus on individual phospholipids present in A549 membranes. As PC is the dominant phospholipid in cellular membranes, LUVs composed of PC were explored to monitor binding and rupture by silica NPs, with a specific focus on the role of PC in these processes. To determine the dose–response relationship of PC for LUV binding and rupture by silica NPs, mixtures of PC and phosphatidylglycerol (PG) were titrated, as these LUVs can be reliably produced and are stable. Whether only PC, or also the positively charged PE, can promote LUV binding and rupture by silica NPs is not yet known. Hence, PE/PG LUVs were produced for a direct comparison. Finally, molecular dynamics (MD) simulations were used to simulate the interaction of single phospholipids (PC, PE) with silica NPs. In these simulations, the relative importance of charged and neutral silanol groups in the interaction with PC and PE was addressed. This is an important consideration, as during endocytosis of particles, the pH drops significantly, which may further promote the detrimental interaction of silica particles with endolysosomal membranes.

## 2. Results

### 2.1. Physicochemical Characterization of Silica (SiO<sub>2</sub>) NPs

Commercial colloidal SiO<sub>2</sub>-NPs were prepared by the Stöber synthesis to produce amorphous colloidal particles of different sizes (Table 1). The primary size was determined by transmission electron microscopy, while the hydrodynamic size in water, cell culture medium, and vesicle assay buffer was measured by dynamic light scattering (DLS). The relative charge of particles is reflected by the zeta potential. As protein adsorption to silica NPs has been shown to reduce cytotoxicity<sup>[20,41]</sup> and interaction

with phospholipid bilayers and vesicles,<sup>[30,33]</sup> we also pre-coated particles by incubation in cell culture medium (Dulbecco's modified Eagle's medium (DMEM)) containing 10% fetal bovine serum (FBS). After centrifugation, the pellet was resuspended in DMEM without FBS. In addition to colloidal silica NPs, we studied Aerosil200, which are silica particles produced by flame synthesis and are widely used in industry. The surface properties of such so-called pyrogenic or fumed silica NPs differ from colloidal silica NPs synthesized, e.g., by the Stöber method.<sup>[42]</sup> The high temperature during the synthesis of pyrogenic silica reduces the number of silanol groups due to dehydration and increases the amount of strained three-membered siloxane rings. Homolytic cleavage of these rings can trigger the production of reactive oxygen species.<sup>[15,42]</sup> Therefore, we wanted to compare the interaction of phospholipid vesicles and silica NPs with different surface properties produced by the main synthesis routes. According to the manufacturer, the nominal particle size and specific surface area (SSA) of Aerosil200 are 12 nm and 200 ± 25 m<sup>2</sup> g<sup>-1</sup>, respectively. Previously, we used transmission electron microscopy (TEM) to study the size distribution, morphology, and aggregation of Aerosil200. These NPs are nearly spherical, with variable primary particle sizes, and form larger aggregates.<sup>[19]</sup> The measured primary particle size of the colloidal SiO<sub>2</sub>-70 nm NPs was 55 ± 7 nm, as determined by TEM analysis, and the calculated SSA was 55 m<sup>2</sup> g<sup>-1</sup>. Similar values were obtained for carboxylated SiO<sub>2</sub>-70 nm NPs, with a primary size of 64 ± 7 nm and an SSA of 47 m<sup>2</sup> g<sup>-1</sup>. To evaluate the impact of particle size on vesicle interaction, SiO<sub>2</sub>-500 nm microparticles (MPs) were also included in the analysis, with a primary size of 433 ± 25 nm and an SSA of 6.9 m<sup>2</sup> g<sup>-1</sup>.

DLS measurements after 6 and 24 h revealed the presence of larger aggregates of Aerosil200 suspended in cell

**Table 1.** Characterization of the various silica particles. The primary size of particles was determined by transmission electron microscopy (TEM). The hydrodynamic diameters ( $d_H$ ) of fumed silica NPs (Aerosil200) and colloidal silica particles (SiO<sub>2</sub>-70 nm, SiO<sub>2</sub>-COOH-70 nm, and SiO<sub>2</sub>-500 nm) were analyzed in cell culture medium (DMEM) or assay buffer (HEPES-NaCl 150 × 10<sup>-3</sup> M, pH 7.5) by DLS (dynamic light scattering). Plain silica NPs were also pre-coated as a control (mock) in DMEM or with proteins (10% FBS/DMEM) and analyzed after centrifugation and resuspension in assay buffer. Particle suspensions at a particle concentration of 50–100 μg mL<sup>-1</sup> were incubated at 37 °C and 5% CO<sub>2</sub> for the indicated time points and vortexed directly before measurement. Depicted is the size derived from the intensity distribution as means ± SD and the polydispersity index (PDI) from three up to six measurements.

Particle	Nominal primary particle diameter [nm]	TEM [nm]	Specific surface area [m <sup>2</sup> g <sup>-1</sup> ]	Zeta potential [mV]	DLS			
					Medium and pre-coating	Time [h]	$d_H$ [nm]	PDI
Aerosil200	12 <sup>a)</sup>	15 ± 10 <sup>b)</sup>	200 ± 25 <sup>a)</sup>	-33 ± 3 <sup>e)</sup>	DMEM	24	232 ± 8 <sup>e)</sup>	0.2 ± 0.01 <sup>e)</sup>
					HEPES-NaCl	0.5	324 ± 27	0.23 ± 0.01
SiO <sub>2</sub> -70nm	70 <sup>a)</sup>	55 ± 7 <sup>c)</sup>	55 <sup>d)</sup>	-38 ± 1 <sup>e)</sup>	DMEM	24	51 ± 0.4 <sup>e)</sup>	0.08 ± 0.003 <sup>e)</sup>
					mock	24	70 ± 2 <sup>e)</sup>	0.06 ± 0.02 <sup>e)</sup>
					FBS	24	286 ± 125 <sup>e)</sup>	0.5 ± 0.06 <sup>e)</sup>
					HEPES-NaCl	0.5	62 ± 0.3	0.03 ± 0.004
SiO <sub>2</sub> -COOH-70nm	70 <sup>a)</sup>	64 ± 7 <sup>d)</sup>	47 <sup>d)</sup>	-32 ± 11	DMEM	24	100 ± 2	0.42 ± 0.1
					HEPES-NaCl	0.5	67 ± 1	0.04 ± 0.02
SiO <sub>2</sub> -500nm	500 <sup>a)</sup>	433 ± 25 <sup>d)</sup>	7 <sup>d)</sup>	-41 ± 2	DMEM	24	505 ± 28	0.07 ± 0.06
					HEPES-NaCl	0.5	527 ± 7	0.13 ± 0.02

<sup>a)</sup>Data provided by the supplier, already published in; <sup>b)</sup>Mülhopt et al. (2018); <sup>c)</sup>Hsiao et al. (2019); <sup>d)</sup>Fritsch-Decker et al. (2019); <sup>e)</sup>Leibe et al. (2019).

culture medium (DMEM), consistent with our previous findings.<sup>[19]</sup> Similar sizes were recorded when Aerosil200 was suspended in the assay buffer used to study NP interactions with lipid vesicles. The SiO<sub>2</sub>-70 nm NPs and SiO<sub>2</sub>-500 nm MPs were found to be nearly monodispersed when suspended in assay buffer or DMEM, with a diameter close to the nominal diameter provided by the manufacturer, i.e., ≈50–70 and 520 nm, respectively. However, pre-incubation with FBS and subsequent resuspension in DMEM increased the size of SiO<sub>2</sub>-70 nm NPs, possibly due to the formation of a protein corona, as well as slight agglomeration resulting from several rounds of centrifugation, which may facilitate particle interactions. Finally, the zeta potential of the selected NPs was negative and below –30 mV, as expected for silica. Furthermore, coating of the SiO<sub>2</sub>-70 nm NPs only slightly reduced the zeta potential (Table S1, Supporting Information).

## 2.2. Interaction of SiO<sub>2</sub>-NPs with Human Lung Epithelial Cells and LUVs Composed of the Main Cellular Membrane Phospholipids

LUVs were created with a phospholipid composition partially similar to that of human A549 lung epithelial cells, with the following percentage of PC (55%), PE (25%), SM (5%), and PS (15%).<sup>[40]</sup> The PS concentration was higher than the measured 5% in the cellular membrane fractions because other phospholipids comprising the remaining 10% (such as diphosphatidylglycerol, lyso(bis)phosphatidic acid, phosphatidylinositol, and others) were not included for simplicity (Table S2, Supporting Information). These dye-loaded LUVs of about 120 nm diameter (Figure S3b, Supporting Information) were incubated with various silica NPs. Fluorescent dye release upon LUV permeabilization served as a direct read-out for membranolysis (Figure 1a and Figure S1, Supporting Information). Colloidal or fumed

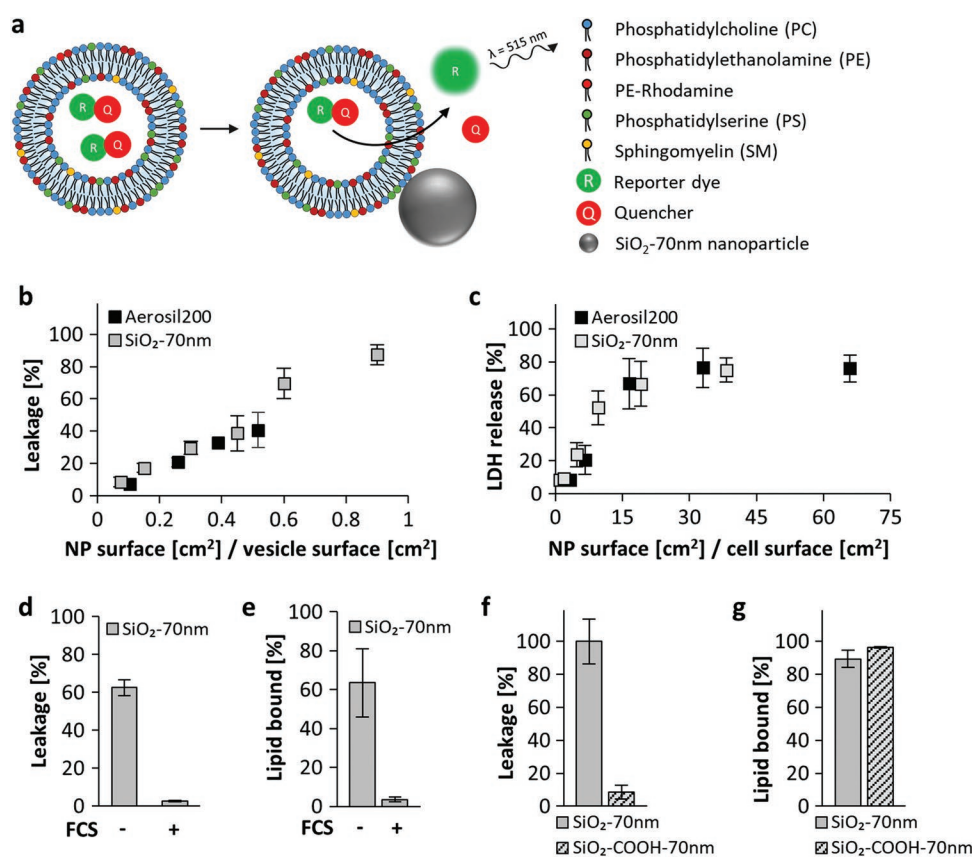


**Figure 1.** Rupture of phospholipid vesicles recapitulates membranolysis by silica nanoparticles (NPs). a) Schematic representation of the experimental layout, using large unilamellar vesicles (LUVs) with a phospholipid composition resembling human A549 lung epithelial membranes: 55% PC (blue), 25% PE (dark red), 15% PS (green), and 5% SM (yellow). LUVs were spiked with rhodamine-labeled PE (bright red) for quantification of binding to NPs. Trapped inside the LUVs are a reporter dye (R, green) and a quencher (Q, red). Membranolysis upon contact with SiO<sub>2</sub> nanoparticles (gray) enables the release of reporter and quencher molecules, as evidenced by enhanced fluorescence of the free reporter dye. b) Both, fumed and colloidal SiO<sub>2</sub>-NPs cause surface area-dependent rupture of LUVs, as well as of (c), membranes in A549 human lung epithelial cells, with similar efficiency. Given are the means ± MAD (*n* = 2) or the means ± SD (*n* = 3–5) in (b) or the means ± SD (*n* = 3–7) in (c). d) Surface coating by protein adsorption (fetal calf serum, FCS) of colloidal SiO<sub>2</sub>-70 nm NPs (0.3 cm<sup>2</sup> NP surface cm<sup>-2</sup> LUV surface) prevents the rupture of LUVs. e) Protein adsorption prevents binding of NPs to LUVs. f,g) Surface carboxylation of SiO<sub>2</sub> NPs (SiO<sub>2</sub>-COOH-70 nm) suppresses rupture of, but not binding to, LUVs. d–g) Dye leakage and binding of LUVs by protein coated, pristine and carboxylated NPs are expressed as relative percentage of the respective control values, which were set to 100%. Given are the means ± MAD (*n* = 2) in (d, f) or the means ± SD (*n* = 4) in (e, g). For the cellular and dye leakage assays, the detergent Triton X-100 was used as a control for complete lysis, whereas lipid binding to NPs was normalized to the lipid content of untreated LUVs.

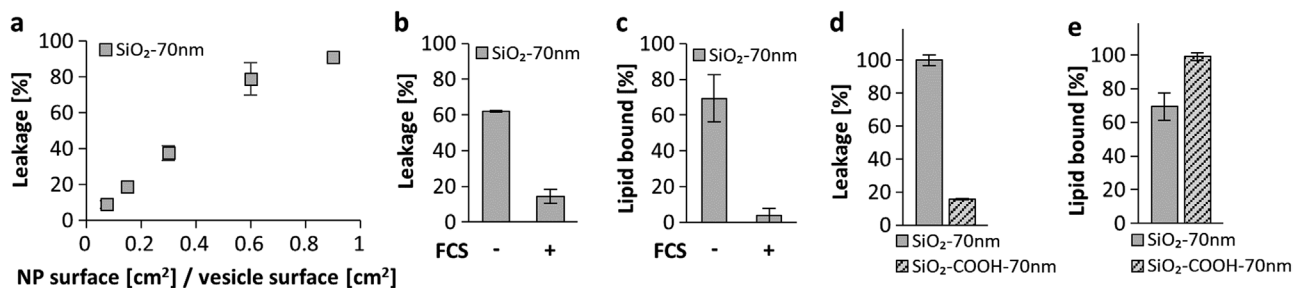


**Figure 2.** PC is sufficient for lysis of LUVs by SiO<sub>2</sub>-NPs. a) LUVs composed solely of phosphatidylcholine (POPC) are lysed by SiO<sub>2</sub>-70 nm NPs. Given are the means  $\pm$  MAD ( $n = 2$ ) or the mean  $\pm$  SD ( $n = 4$ ). b) Surface coating of SiO<sub>2</sub>-NPs by protein adsorption prevents the rupture (given is the mean  $\pm$  SD,  $n = 4$ , -FCS samples or the mean  $\pm$  MAD,  $n = 2$ , +FCS samples) and c) binding of LUVs composed of PC (given are the means  $\pm$  SD,  $n = 4$ ). d,e) Surface carboxylation of SiO<sub>2</sub> NPs (SiO<sub>2</sub>-COOH-70 nm) suppresses rupture of, but not binding to, LUVs. Given are the means  $\pm$  MAD,  $n = 2$ , in (d) or the means  $\pm$  SD,  $n = 4$ , in (e). b–e) Dye leakage and binding of LUVs by protein coated and pristine NPs are expressed as relative percentage of the respective control values which were set to 100%.

SiO<sub>2</sub>-NPs triggered lysis with similar efficiency (Figure S1, Supporting Information), and the degree of lysis correlated with the surface area of the NPs (Figure 1b). Of note, binding of LUVs to SiO<sub>2</sub>-NPs required a lower particle number concentration than LUV rupture, indicating that multiple NPs interacted with a single vesicle to trigger leakage (Figure S2, Supporting Information). This finding was supported by DLS measurements, where at increasing NP/LUV ratios an increase in size correlated with enhanced leakage (Figure S3, Supporting Information). For comparison, membranolysis was also monitored in living A549 cells, and both types of SiO<sub>2</sub>-NP disturbed the membrane integrity, indicated by release of lactate dehydrogenase (LDH). However, a higher specific surface area dose was required, possibly due to the lack of shear forces applied during the stirred LUV assay (Figure 1c). Interestingly, the adsorption of serum proteins to the SiO<sub>2</sub>-NPs prevented LUV binding and rupture (Figure 1d,e), as well as cell membrane damage in A549 cells (Figure S4a, Supporting Information). Furthermore, carboxylated SiO<sub>2</sub>-NPs were found to be inefficient in triggering dye release from LUVs, despite being able to bind to LUVs (Figure 1f,g). The absence of LUV rupture was in line with the low cytotoxicity measured by LDH release from A549 cells upon exposure to these carboxylated SiO<sub>2</sub>-NPs (Figure S4b, Supporting Information). Hence, it can be concluded that LUVs with a phospholipid composition that partially mimics that of membranes extracted from lung epithelial cells are suitable models to assess membrane damage induced by different types of SiO<sub>2</sub>-NPs.

### 2.3. Probing the Role of the Individual Phospholipids PC, PE, and SM for LUV Binding to and Rupture by Silica NPs

In contrast to previous studies where liposomes composed of nonphysiological or a fixed ratio of physiological lipids were used to demonstrate vesicle binding to and rupture by various nanomaterials, including nanosilica,<sup>[33,43,44]</sup> our goal was to selectively investigate the requirement of specific lipid head groups, as found in lung epithelia and other target cells, and examine their role in membranolysis. With a reliable assay established to study NP interaction with phospholipid membranes of physiologically relevant composition that resemble

cellular membranes, we next asked which of these specific phospholipids is required for binding to and rupture by SiO<sub>2</sub>-NPs. Positively charged tetra-alkyl ammonium head groups, as present in PC and SM, have been postulated as key target sites.<sup>[22,45,46]</sup> Since both phospholipids constitute roughly 60% of the total phospholipid content of A549 cellular membranes and the LUVs used above, we tested whether PC alone would be sufficient to promote leakage of vesicles. Indeed, LUVs composed of pure PC readily disintegrated after SiO<sub>2</sub>-NP exposure, similar to the mixed LUVs resembling cellular membranes (Figure 2a). Again, surface coating of the SiO<sub>2</sub>-NPs by serum interfered with the response (Figure 2b) and impaired their binding to the PC lipid vesicles (Figure 2c). Carboxyl groups on the silica surface also reduced dye leakage compared to plain silica NPs (Figure 2d), but carboxylated SiO<sub>2</sub> NPs still strongly bound to the PC LUVs (Figure 2e). Given that an increased surface curvature of silica nano- versus microparticles could augment the disturbance of lipid vesicles, we compared the effects of 70 and 500 nm sized SiO<sub>2</sub> particles (Figure S5, Supporting Information). LUVs resembling either cellular membranes or entirely composed of PC were lysed with similar efficiency by both nano- and microparticles in proportion to the surface area dose. Therefore, the available surface area on the silica particles appears to be the critical parameter driving the disturbance of phospholipid bilayers in LUVs.

At this point of the study, we must note that the detrimental interplay of SiO<sub>2</sub>-NPs with LUVs may not necessarily depend solely on PC, because all major binding forces such as hydrogen-bonding with oxygen or nitrogen atoms, hydrophobic, and electrostatic interactions should also be present in other membrane phospholipids. To examine the role of different lipid head groups, we prepared a set of LUVs in which zwitterionic PC was gradually exchanged by the negatively charged PG. In this series, leakage is seen to be reduced in a dose-dependent manner (Figure 3a). This effect could be attributed to either electrostatic repulsion of negatively charged SiO<sub>2</sub>-NPs with a zeta potential of  $-38$  mV (Table 1) by anionic PG, or to the absence of quaternary PC head groups. Another set of LUVs was prepared from PE and PG at the same ratios as above. These vesicles remained fully intact in the presence of SiO<sub>2</sub>-NPs (Figure 3b), demonstrating the specific role of the choline head group for vesicle rupture.

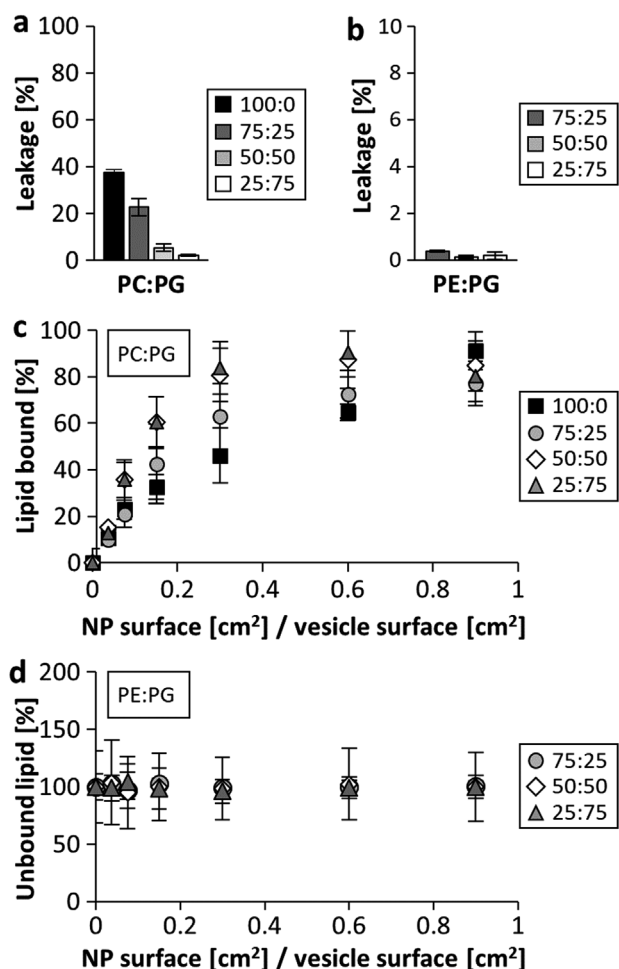


**Figure 3.** Quaternary ammonium head groups are essential and sufficient for lysis of and binding to LUVs by silica NPs. a) Increasing amounts of PC, b) but not phosphatidylethanolamine (PE) versus phosphatidylglycerol (PG), facilitate rupture of composite LUVs by SiO<sub>2</sub>-70 nm (0.3 cm<sup>2</sup> cm<sup>-2</sup>). c) PC, but not d) PE-containing composite LUVs bind efficiently to SiO<sub>2</sub>-70 nm NPs. Values were normalized to the respective control, which were set to 100%. Given are the means ± MAD, *n* = 2, in (a–c) or the means ± SD, *n* = 4, in (d).

Next, we analyzed whether SiO<sub>2</sub>-NPs would bind preferentially to LUVs containing PC with a quaternary ammonium head group, compared to PE with a primary amine. The different vulnerability of these two types of LUV was indeed explained by such differential affinity. In contrast to PC/PG LUVs, binding of PE/PG LUVs by SiO<sub>2</sub>-NPs was almost absent (Figure 3c,d). This finding shows that the PC head group is indeed necessary to promote binding of silica NPs to LUVs. Of note, although reducing the amount of PC renders vesicles resistant to lysis (Figure 3a), binding of LUVs to SiO<sub>2</sub>-NPs was not impaired by increased levels of negatively charged PG (Figure 3c). The apparent decreased binding of LUVs composed only of PC versus those containing in addition PG is most likely explained by LUV lysis, which leads to additional accessibility of the inner leaflet of the membrane. Indeed, when the percentage of lysed LUVs and the additional available surface area is factored in, the relative difference in binding of PC LUVs is compensated (Figure S6, Supporting Information). Thus, on

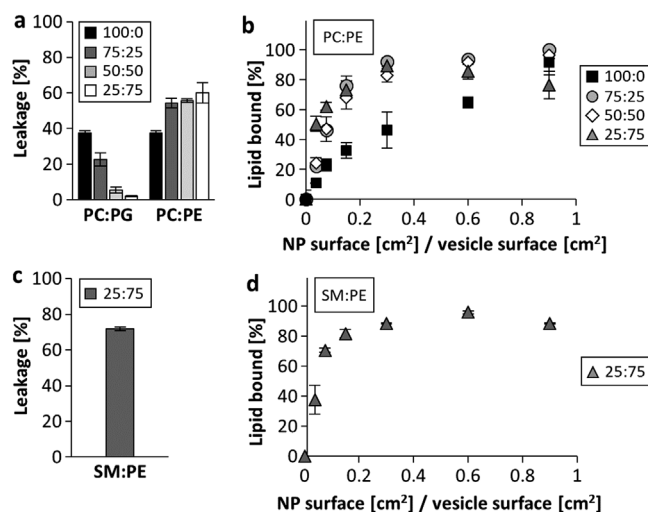


**Figure 4.** Increase of the overall net charge by phosphatidylethanolamine enhances LUV leakage induced by SiO<sub>2</sub>-NPs dependent on quaternary ammonium head groups. a) PE enhances LUV rupture dependent on PC. LUVs with different molar ratios of PC and PE were incubated with SiO<sub>2</sub>-70 nm NPs (0.3 cm<sup>2</sup> cm<sup>-2</sup>). b) PC:PE LUVs bind to SiO<sub>2</sub>-70 nm NPs with enhanced efficiency compared to PC:PG LUVs (see Figure 3c). c,d) The quaternary ammonium head groups in sphingomyelin (SM) also promote lysis of LUVs by SiO<sub>2</sub>-70 nm NPs (0.3 cm<sup>2</sup> cm<sup>-2</sup>) and enhanced binding to LUVs. Values were normalized to the respective control, which were set to 100%. Given are the means ± MAD (*n* = 2).

top of binding LUVs by SiO<sub>2</sub>-NPs, a higher threshold of PC is needed for rupture to occur. To interrogate any electrostatic effects exerted by anionic PG, yet another set of LUVs was prepared using instead zwitterionic PE, in order to generate uncharged PC/PE vesicles. These lipid vesicles demonstrated even enhanced leakage by SiO<sub>2</sub>-NPs (Figure 4a) as well as binding (Figures 4b and 3c). As the quaternary ammonium head group of PC is also found in SM, we additionally investigated SM-containing LUVs. In fact, also SM promotes the binding of LUVs to and rupture by SiO<sub>2</sub>-NPs (Figure 4c,d). Overall, the quaternary ammonium groups in the membrane phospholipids PC and SM enable bonding with SiO<sub>2</sub>-NPs, as a condition sine qua non. Binding of SiO<sub>2</sub>-NPs to LUVs via PC appears to be further enhanced by the presence of PE. However, PE is not able to promote interaction of SiO<sub>2</sub>-NPs with all LUVs composed of various ratios of PE/PG. Therefore, even at neutral pH, the primary amine group of PE with a pK<sub>a</sub> value around 9.6<sup>[47]</sup> cannot substitute for the permanently charged choline group in PC to facilitate silica binding per se. As a further control, titania NPs, in contrast to SiO<sub>2</sub>-NPs, did not provoke lysis of PC LUVs (Figure S7, Supporting Information), highlighting the specific interaction between the silica surface and the PC head group.

#### 2.4. Simulation of the Interaction of PE and PC with a Flat Silica Surface Reveal Preferential Binding of PC Dependent on the pH Level

Finally, MD simulations were used to gain a better understanding of the interaction of single phospholipids PE and PC with silica. Whereas a number of other studies employed phospholipid

bilayer models that were exposed to silica clusters, we took the reverse approach, allowing a flat silica surface to interact with PC and PE. We also focused on the relative importance of charged and neutral silanol groups in these interactions, a topic which has not been addressed in detail so far.<sup>[48–50]</sup> Previously, it has been shown that silica NPs contain at least two types of silanol groups at the surface, with  $pK_a$  values between 4.5–5.5 and 8.5–9.9, and a relative percentage of about 17% and 83%, respectively. The point of zero charge (pzc) for silica is between pH 2 and 4.<sup>[51]</sup> Here, the silica surface was modeled with a surface density of 4.7 silanol groups  $\text{nm}^{-2}$ , which were either fully protonated or partially deprotonated, as previously described, at a physiologically relevant pH of either 4.0 or 7.0 (as found in the endolysosomal compartment or cytoplasm, respectively), and its interaction with PC and PE was calculated (Figure S8, Supporting Information).<sup>[21,52]</sup> In support of the empirical studies above, the binding energy between the silica surface and PC was increased compared to PE, especially in the case of protonated silanol groups (Figure 5a). Repulsive forces were recorded between negatively charged PG and the deprotonated silica surface, which fits well with our experimental data on increased binding of the mixed PC vesicles in which the PG component was replaced by PE (Figure 4b). Spatiotemporal analysis of the molecular interaction revealed no preferential localization of the nitrogen, oxygen, and phosphorus atoms of PC at protonated or deprotonated silanol groups (Figure 5b and Figure S9a, Supporting Information). In contrast, PE predominantly interacted with the charged silanol groups, as evidenced by the closest proximity and binding frequency of the nitrogen atom, while the oxygen and phosphorus atoms were observed at a greater distance (Figure 5c and Figure S9b, Supporting Information). Thus, zwitterionic PC interacts with the silica surface by hydrogen bonding of the oxygen atoms in its phosphate group with protonated silanol groups (Table S4, Supporting Information), which is in line with recent MD simulations.<sup>[53]</sup> Zwitterionic PE, on the other hand, binds electrostatically to deprotonated silanols via its cationic amino group (Table S4a, Supporting Information), consistent with the increased binding energy observed for the deprotonated versus protonated silica surface (Figure 5a).

### 3. Discussion

#### 3.1. Role of PC and PE in the Interaction of LUVs with Silica NPs

Previous studies investigated the impact of NPs on lipid vesicles composed of 100% PC or an arbitrary mixture of PC and some other phospholipids without considering the physiological composition of cellular membranes. However, in this study, we decided to produce LUVs with a similar percentage of PC, PE, and SM as determined in membranes derived from A549 cells, an established model to assess the impact of nanoparticles. The relative percentage of phospholipids as determined for A549 lung carcinoma cells is very similar to cultured, normal lung epithelial cells isolated from rat and feline lungs.<sup>[40]</sup> Thus, we show that LUVs with a more physiological membrane composition relevant for the target cells (in our case lung epithelial cells) can be used to study the impact of nanoparticles instead of relying on LUVs with an artificial and nonphysiological composition. Whereas PC

constitutes  $\approx 50\%$  of A549 cellular membrane lipids, PE still contributes another 25% to the total amount of lipids.<sup>[40]</sup> However, studying vesicles composed of different ratios of either PC/PG or PE/PG, only in the presence of PC binding to silica NPs was observed. Thus, PC mediates binding of silica NPs to phospholipid vesicles and on top is also the dominant phospholipid in cellular membranes. For PC/PG vesicles, lysis became apparent at a concentration of 50% PC, although full binding to silica NPs was still measured at 25% PC. Thus, a certain threshold of PC in phospholipid bilayers is needed for vesicle rupture to occur, which may explain the vulnerability of cellular membranes due to their relatively high content of PC. As so far in the literature most often vesicles (SUVs, LUVs, GUVs) with a fixed PC content were used, the relative PC content was not systematically titrated and thus the concentration-dependent effect of PC on binding and rupture has not been explored. Additionally, the synergistic action of PC and PE in LUV binding and rupture, as observed in the present work, was not studied before. Surface modification by carboxyl groups still allowed binding of silica NPs to LUVs but prevented membranolysis. However, in case of protein adsorption, neither binding of nor rupture by silica NPs could be detected. In accordance with previous models to explain deleterious interactions of silica NPs and other nanomaterials,<sup>[32,54]</sup> we propose an adapted three-step process whereby silica NPs i) first bind to LUVs and subsequently, dependent on the PC and PE content and thus bond intensity, lead to ii) vesicle deformation, culminating in the iii) formation of an SLB coinciding with LUV rupture (Figure 6). Whereas in case of protein adsorption, the interaction of silica NPs with LUVs is entirely abrogated, surface carboxylation still allows for binding but either due to steric hindrance or reduction of critical silanol surface groups, the formation of an SLB may be inhibited. A similar observation was made for PEGylated amine-modified silica NPs, where coupling of polyethylene glycol (PEG) molecules to the amine groups reduced lysis of LUVs.<sup>[29]</sup> Several comparative studies have investigated the mechanism of binding to LUVs composed of PC by titania and silica NPs.<sup>[54–57]</sup> Silica NPs are suggested to interact via charged silanol groups with the choline head group of PC, enabling binding and subsequently the formation of an SLB. In contrast, titania NPs form covalent bonds with the phosphate group in PC, and although they interact even more strongly with PC, they do not trigger LUV lysis, in line with our findings. Steric hindrance by the choline head group has been proposed as a possible explanation, which may prevent formation of an SLB on titania NPs. In the present work, we focused our analysis on the role of PC, SM, and PE in the interaction of LUVs with silica NPs. However, it is important to note that other membrane lipids such as PS, diphosphatidylglycerol, lyso(bis)phosphatidic acid, phosphatidylinositol, and cholesterol, should also be studied in such a systematic way in the future to obtain a complete understanding concerning the relevance of individual lipids for membranolysis provoked by silica particles.

#### 3.2. Impact of Protein Adsorption and Membrane Proteins on the Membranolytic Activity of Silica NPs

In previous studies, we have already shown that purification of Aerosil200 and colloidal 70 nm silica NPs in the presence of FBS leads to surface binding of mainly apolipoproteins,

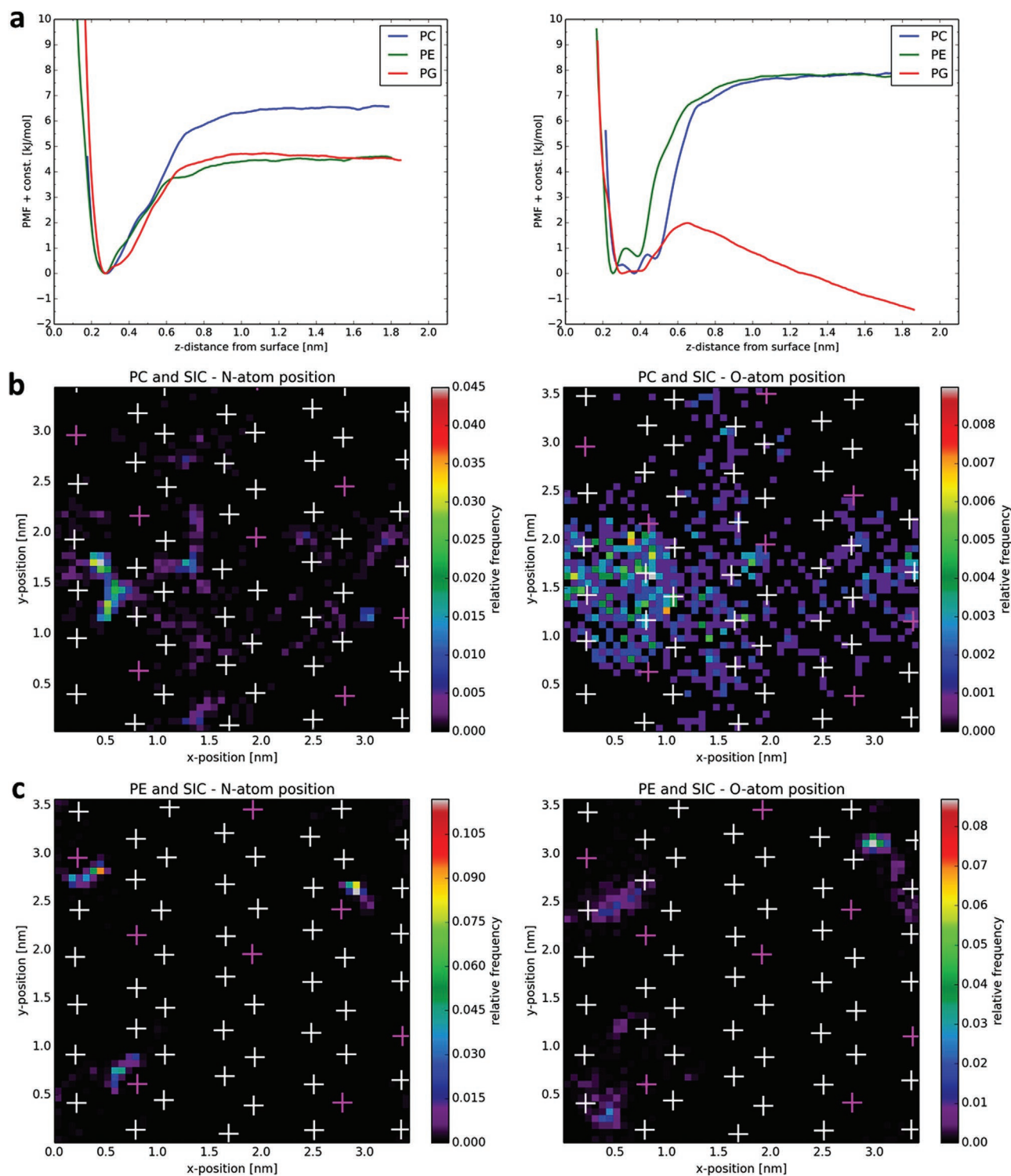


**Figure 5.** Molecular modeling reveals increased binding energy of PC to the silica surface, but no preferential localization at protonated or deprotonated silanols. a) Compared to PE and PG, PC exhibits the highest binding energy to the silica surface which in the model is either fully protonated (left panel) or partially deprotonated (right panel). b) N- and O-atoms of PC show no preferential localization at protonated or deprotonated silanol groups. c) N- and O-atoms of PE are most frequently localized to ionized silanol groups. Crosses indicate positions of deprotonated (pink) and protonated (white) silanol groups.

complement factors, and some other serum proteins.<sup>[58,59]</sup> This is in line with similar studies characterizing the protein corona of colloidal silica nanoparticles exposed to human plasma.<sup>[20]</sup>

The coating of particles with such serum proteins may inhibit the direct interaction of the silica surface with phospholipid membranes, thereby preventing the disturbance of membrane

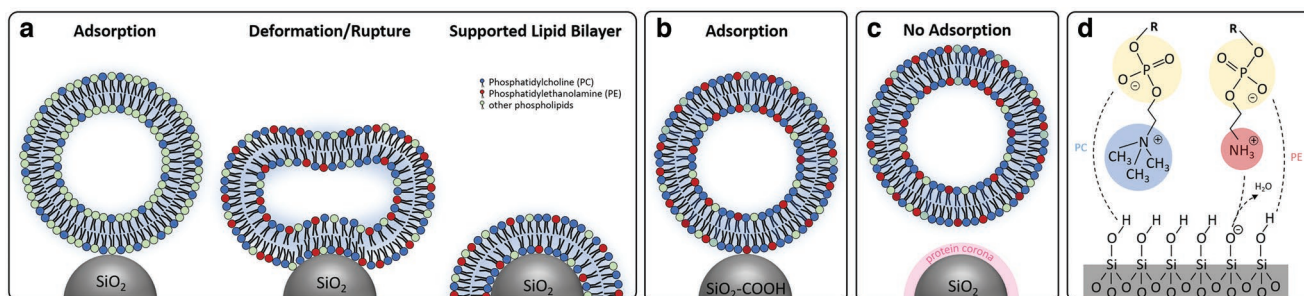


**Figure 6.** Model of membranolytic activity of silica NPs. a) Silica NPs bind to large unilamellar vesicles (LUV) dependent on phospholipids bearing a choline head group (e.g., PC). However, only at a higher and critical percentage of PC, LUVs are ruptured, a process which is further facilitated by the presence of PE. The final step results in formation of an SLB, as previously shown by others. b) Whereas surface carboxylation of silica NPs still allows binding, but not rupture, of LUVs, c) protein adsorption entirely suppresses both processes. d) Molecular modeling and experimental data indicate a critical role and threshold of PC to promote binding to and rupture by silica NPs via hydrogen bonding, which is further enhanced by electrostatic interactions with PE.

integrity, as previously suggested.<sup>[30]</sup> Whereas pristine silica particles accumulate at the surface of epithelial cells and macrophages in the absence of serum and provoke membranolytic, serum-precoated silica particles are endocytosed by epithelial cells without any concomitant signs of cell damage.<sup>[41]</sup> However, engulfment of silica particles in the presence of serum still leads to cell death via lysosomal injury in macrophages, as presumably the protein corona on the particle surface is gradually degraded, thereby exposing silica surface groups to endolysosomal membranes.<sup>[60]</sup>

In the present study, we incubated A549 cells with silica NPs in the absence of serum to assess membranolytic activity. Upon inhalation, NPs encounter macrophages and lung epithelial cells at the air-liquid interphase, where cells are covered by the lung lining fluid, which has a much lower protein content compared to blood plasma or serum. Therefore, exposure of cells *in vitro* in the presence of high levels of serum proteins (10% FBS) does not closely mimic the physiological conditions in the lung. In toxicological studies addressing the impact of NPs on lung cells, it is now appreciated that during the exposure to NPs, the amount of serum in the exposure medium should be reduced, as the formation of a protein corona might artificially suppress toxicity. In fact, *in vitro* experiments with alveolar macrophages cultivated in the absence of serum have been shown to more accurately predict the short-term inhalation toxicity *in vivo* for 18 different nanomaterials, including silica NPs.<sup>[61]</sup>

As silica NPs accumulate at the membrane of A549 cells in the absence of serum, as visualized by fluorescence imaging and electron microscopy,<sup>[41]</sup> the pristine silica surface of particles may directly interact with the phospholipids of the outer cell membrane, causing dose-dependent membrane damage. Nevertheless, this hypothesis does not exclude other adverse effects of silica particles, which are essential for the cytotoxic response. Membrane rupture in cells can also be the consequence of more complex signaling events provoked by silica NPs, which are still incompletely understood. Specifically, the primary or so-called molecular initiating events triggering cell death have not been identified. Indeed, by employing LUVs composed only of phospholipids, the importance of membrane proteins in the process of membrane rupture is not considered. As an example, knock-out of scavenger receptor B1 (SR-B1) in macrophages reduces tethering of silica particles to and

LDH leakage from murine macrophages. Currently, the molecular mechanism by which SR-B1 might promote cell death in response to silica particles is unclear. Although SR-B1 does not promote internalization of silica particles, it might either trigger signaling cascades important for cell death or alternatively increase the interaction with phospholipids in the membrane. Little is known about which proteins, dependent on cell type, are involved in cytotoxicity provoked by silica particles. To this end, genetical or chemical screens could be performed to elucidate the role of different proteins and address their mechanism of action, particularly their role in membrane damage. Incorporation of such target proteins, e.g., SR-B1, into GUVs producing proteovesicles<sup>[27]</sup> might help to more directly assess the interaction of silica particles with phospholipids and membrane proteins in the context of membranolytic activity.

In addition to considering the role of membrane proteins in vesicle binding and rupture induced by silica NPs, the relevance of membrane curvature needs to be addressed in future experiments in more detail. The adhesion energy between NPs and vesicle membranes defines their interaction and wrapping by phospholipids, which is opposed by the resistance of the membrane to deformation.<sup>[62]</sup> As shown for GUVs, the relative membrane curvature and the size of silica particles are important factors in determining whether vesicle fusion or rupture occurs. While GUVs are similar in size to cells, LUVs and SUVs are more comparable to intracellular membrane compartments, such as endolysosomal vesicles, which have a much higher membrane curvature. When particles approach cells, they first encounter the outer cell membrane, and upon endocytosis, become engulfed. During this process, membrane curvature increases, which may be an important parameter to define in which cellular compartment the membrane is ultimately damaged.

### 3.3. Molecular Dynamics Simulations to Improve Our Understanding of the Interaction of Silica NPs with Cellular Membranes

In our MD simulations, we studied the interaction of single phospholipids with a flat silica surface, which differs from previous studies that used phospholipid bilayer models exposed to

silica clusters of about 1 nm.<sup>[48–50]</sup> Yuan and colleagues investigated the interaction of silica clusters with dipalmitoylphosphatidylcholine, a component of alveolar lung surfactant, and found that silica clusters showed a stronger binding to the P-atom of the phosphate group than to the N-atom of the choline head group. Van der Waals forces and hydrogen bonding were suggested to contribute to the binding, leading to the fixation of the phosphate head group and thereby decreasing bilayer fluidity. Hydrogen bonding of the phosphate group within POPC with the protonated silanol group of silica nanoclusters was also analyzed in another study, where no significant numbers of hydrogen bonds between the surface and the head groups were detected.<sup>[48]</sup> The specific role of hydrogen bonding on the basis of cluster simulations remains unclear, because the integration of the cluster into the membrane necessarily leads to intermediate configurations where hydrogen bond donors and acceptors are in close proximity. This observation alone is not proof that hydrogen bonding is the dominant form for the interaction of the cluster with the membrane. In a bilayer model composed of PC, PE, and phosphoinositide, interaction with silica nanoclusters decreased the fluidity.<sup>[49]</sup> Whereas the NH<sub>3</sub><sup>+</sup> terminal group of PE formed stable hydrogen bonds with silica, in case of PC, only transient hydrogen bonds were initially established between the choline head groups and the silanols. Subsequently, stronger binding to the middle phosphate group in PC was observed, which also more drastically restrained phospholipid mobility, resulting in local gelation. The latter study suggested that the interaction of silanols with PC, compared to PE, leads to a stronger reduction of membrane fluidity.

The simulation of phospholipid bilayers may also be suited to integrate lipid rafts in more complex 2D and 3D membrane models to study their relevance for the interactions with silica NPs. Experimentally, SLBs can be engineered with segregated domains containing enhanced levels of SM and cholesterol, to which increased binding of gold NPs could be shown.<sup>[63]</sup> In our modeling studies, we addressed the relative importance of charged and neutral silanol groups in the interaction with PC and PE. Whereas protonated neutral silanol groups appear to enhance binding to PC compared to charged silanols, PE preferentially binds to negatively charged silanol groups. The impact of the relative charge of silanols on the interaction with membrane phospholipids has not been extensively studied, but is quite important, as during endocytosis of particles, the pH drops from about 7 to 4, which could further promote the detrimental interaction of silica particles with endolysosomal membranes.

The MD simulations discussed above provide a theoretical basis for the molecular interactions observed experimentally, confirming the key role of PC as a mediator of binding lipid membranes to SiO<sub>2</sub>-NPs that will eventually result in membranolysis. In support of a strong interaction between phosphatidylcholine lipids with the silica surface, immobilization of PC in liposomes due to binding of silica particles has been documented by others as well.<sup>[46]</sup> The latter work also included some modeling studies, in which a four-membered Si–O ring comprised of hydrophobic siloxane bonds and a deprotonated silanol was simulated to interact with either PC or PS. The calculated binding energy of PC to silica was higher than for PS.

Compared to the charged amine group in PS, the zwitterionic choline head group interacted more strongly with the charged silanol due to enhanced electrostatic forces. In addition, enhanced interactions with the siloxanes and a more favorable de-solvation of the methylated amine moiety were suggested to contribute to the preferential interaction of PC with silica. These mechanisms might also contribute to the higher binding forces of PC versus PE to silica, as observed in our studies.

Apart from selective interactions of the silica surface with specific phospholipids, also a more general mechanism of membranolysis has been proposed, whereby van der Waals forces mediate a disruption of the hydration layer around biological membranes.<sup>[44]</sup> However, the latter model fails to explain the specific requirement of PC or SM for lipid vesicle adsorption and rupture. Therefore, such unspecific phospholipid interactions might rather in addition facilitate membranolysis. At the cellular level, SiO<sub>2</sub>-NPs first interact with the cell membrane and are then taken up by endocytosis, ending up in the endolysosomal compartment. Notably, there is an asymmetric distribution of phospholipids in membranes, particularly of those bearing quaternary ammonium head groups such as SM and PC. These uncharged lipids are preferentially localized in the outer leaflet of the plasma membrane and on the luminal side of endosomal membranes.<sup>[64]</sup> Once SiO<sub>2</sub>-NPs enter the endolysosomal compartment, the pH drops from around 7 at the outside of the cell to about 4–5, thus enhancing protonation of the silanol groups. According to our data, enhanced levels of protonated silanols might increase the interactions of the particle surface with the luminal SM and PC, which is further augmented by the presence of PE. In order for such a direct interaction to occur within the endolysosomal compartment, the protein corona needs to be degraded, a process which, however, is at present poorly understood at the molecular level. Nevertheless, such scenario seems to be highly relevant to describe the detrimental effects of SiO<sub>2</sub>-NPs in macrophages that eventually culminate in lysosomal rupture and cell death.<sup>[60]</sup> Therefore, considering the protein corona in MD simulations to assess the impact on particle-phospholipid interactions would be interesting but requires more effort, particularly in the choice of individual proteins or mixtures thereof to be included. Candidates might be selected from previous mass spectrometry analyses which identified specific proteins bound to silica NPs.<sup>[20,58,59]</sup>

As we have shown in the present work, the relative content of PC and SM in the phospholipid bilayer determines binding to and, at a critical threshold, also rupture by SiO<sub>2</sub>-NPs, which is further enhanced by the presence of PE. As the relative levels of PC/SM and PE vary significantly among different sorts of biological membranes within cells but also across cell types and species,<sup>[65]</sup> our findings might be important to also better understand organelle-, organ-, and species-specific toxicity of silica NPs. Clearly, more research is warranted to investigate membrane interactions with different types of nanomaterials and surface properties, to better understand this important initiating event that is not only essential for membranolysis but possibly also for other downstream responses. For example, the oxidation of cholesterol in lipid rafts due to interaction with graphene oxide has been recently linked to neutrophil extracellular trap formation, which could be prevented by antioxidant treatment.<sup>[66]</sup>

Therefore, a detailed understanding of the interactions of nanomaterials with biomembranes at the molecular level is a prerequisite for specifically tuning material surfaces by chemical modification or by stabilizing the protein corona, in order to prevent disturbance of phospholipid bilayers that will eventually lead to membranolysis and disturbance of cellular function.

## 4. Conclusions

By the use of lipid LUVs with well-defined composition, together with molecular modeling, it has been demonstrated that the presence of quaternary ammonium head groups, specifically found in PC and SM, are necessary to mediate binding to silica NPs. A critical threshold of quaternary ammonium head groups is required to ultimately promote membranolysis by silica NPs (as summarized in Figure 6). These studies not only provide fundamental insights into the mechanism of action of the most abundant class of nanomaterials, SiO<sub>2</sub>-NPs, but will also be very useful to assess membrane interactions of other nanomaterials. Moreover, advanced MD simulations could aid in designing safe nanomaterials based on an improved understanding of their surface interactions with phospholipid bilayers.

## 5. Experimental Section

**Materials: Reagents to prepare LUVs:** The lipids 1-palmitoyl-2-oleoyl-*sn*-glycero-3-phosphocholine (POPC or PC), 1-palmitoyl-2-oleoyl-*sn*-glycero-3-phosphoethanolamine (POPE or PE), 1-palmitoyl-2-oleoyl-*sn*-glycero-3-phosphoserine (POPS or PS), sphingomyelin (brain, Porcine SM), 1-palmitoyl-2-oleoyl-*sn*-glycero-3-phosphoglycerol (POPG or PG), and rhodamine-labeled PE (Rh-PE) were purchased from Avanti Polar Lipids (Alabaster, AL, USA) or from Europe (Grobendonk, Belgium). 8-aminonaphthalene-1,3,6 trisulfonic acid (ANTS), *p*-xylene-bis-pyridinium bromide (DPX) were purchased from Invitrogen (Karlsruhe, Germany), while NaCl, and 4-(2-hydroxyethyl)-1-piperazineethanesulfonic acid (HEPES) were from VWR International GmbH (Bruchsal, Germany).

**Particles:** The TiO<sub>2</sub> nanoparticles (AEROXIDE, P25) were kindly provided by Evonik Industries (Frankfurt, Germany). This material was also used as a reference material of the Organization for Economic Cooperation and Development (OECD) named NM-105. Detailed characteristics of the material are published in Rasmussen et al.<sup>67</sup> Aerosil200 was also provided by Evonik and has been characterized in more detail previously.<sup>68</sup> Colloidal silica NPs were purchased from Postnova Analytics (Landsberg, Germany).

**Cell culture reagents:** The human alveolar type II-like cell line A549<sup>69,70</sup> was obtained from American Type Culture Collection (ATCC, Rockville, MD, US). Cell culture medium DMEM and medium supplements were from ThermoFisher Scientific (Dreieich, Germany). The Cytotoxicity Detection Kit (LDH) was from Sigma (Taufkirchen, Germany).

**Methods: Particle characterization:** To determine the particle size distribution by DLS as well as the zeta potential, a 1 mg mL<sup>-1</sup> stock suspension in deionized water was prepared for all particles as described previously.<sup>141</sup> The stock suspensions were further diluted either in pure DMEM or in HEPES-NaCl 150 × 10<sup>-3</sup> m, pH 7.5. The samples were analyzed after incubation at 37 °C and 5% CO<sub>2</sub> for the indicated time immediately after vortexing using the Zetasizer Nano ZS (Malvern Instruments Ltd., Herrenberg, Germany) at 25 °C and data were processed by the Malvern Zetasizer Nano software. Due to the high conductivity of the cell culture media which led to corrosion of the electrodes (also in accordance with the information provided

by the manufacturer), the zeta potential was assessed in water. Particles were also analyzed by TEM and tested for endotoxins with the chromogenic endpoint Limulus Amebocyte Lysate (LAL) assay (Lonza, Basel, Switzerland), as previously described.<sup>141</sup> The surface area and particle number of colloidal silica nanoparticles were provided by the manufacturer. Briefly, based on the hydrodynamic diameter of spherical silica NPs, the relative surface area and mass per NP could be calculated. The total mass of particles was divided by the individual mass of a silica NP to obtain NP numbers.

**Preparation of the particle suspensions for cell culture and vesicle experiments:** All particle dilutions were prepared freshly by first preparing a 1 mg mL<sup>-1</sup> stock suspension in deionized water. This stock solution was used to prepare the final concentrations of exposure suspensions in either pure DMEM or DMEM containing 10% FBS which were added to the cells. For pre-coating of particles, 100 µg mL<sup>-1</sup> NP suspension was incubated in H<sub>2</sub>O containing 10% FBS for 1 h at 37 °C, while noncoated particles were incubated in H<sub>2</sub>O without FBS supplement. After centrifugation at 18 000 × g at 20 °C for 40 min, the supernatant was discarded, the pellet was washed with H<sub>2</sub>O and centrifuged again at 18 000 × g at 20 °C for 20 min. This pellet was resuspended in the pre-warmed buffer (50 × 10<sup>-3</sup> m NaCl, 10 × 10<sup>-3</sup> m HEPES, pH 7.5) and added to 100 × 10<sup>-6</sup> m LUVs (as mentioned under the Experimental Section membranolysis and binding assay).

**Preparation of LUVs:** The preparation of the LUVs and the membranolysis assay were already described in Wadhvani et al.<sup>71</sup> The lipid powders were dissolved in chloroform and the organic solvent was subsequently removed under a gentle stream of nitrogen, followed by overnight vacuum. To quantify the lipid loss occurring in the vesicle preparation procedure and in the subsequent buffer exchange by gel permeation chromatography, a small amount of Rhodamine-labeled PE (10<sup>-4</sup> molar ratio) was routinely added to the weighed lipid. Lipid dispersions were prepared by the addition of the lipids to reporter dye ANTS and quencher DPX-containing buffer (12.5 × 10<sup>-3</sup> m ANTS, 45 × 10<sup>-3</sup> m DPX, 50 × 10<sup>-3</sup> m NaCl, 10 × 10<sup>-3</sup> m HEPES, pH 7.5). The dispersion was vigorously vortexed (ten times for 1 min) and homogenized with ten freeze-thaw cycles before extrusion through a polycarbonate filter with 100 nm diameter pores (Avanti Mini Extruder, Avanti Polar Lipids, AL, US).

Phospholipid LUVs were prepared with a composition resembling that of human A549 lung epithelial membranes: 55% PC, 25% PE, 15% PS, and 5% SM,<sup>140</sup> as well as traces of Rhodamine-labeled PE for quantification of LUV binding to NPs. Trapped inside the LUVs were the reporter dye and the quencher. The formation of the vesicles was monitored by DLS using the Zetasizer Nano S (Malvern Instruments Ltd., Herrenberg, Germany) at 25 °C. The measurements showed that the multilamellar vesicles had an average diameter of 123 ± 5.7 nm (see also Figure S3, Supporting Information). The surface areas of the LUVs were calculated via the number of phospholipids of the outer leaflet of the membrane and the apl (area per lipid) for each phospholipid composition. Given was the average surface area of 291.3 cm<sup>2</sup> ± 16 cm<sup>2</sup>. The number of LUVs was calculated based on the total amount of used phospholipids divided by the required amount of phospholipids per average vesicle surface area.

**Membranolysis assay:** Membranolysis enabled the release of the fluorescent reporter and quencher molecules inserted in the LUV bilayer after contact with membranolytic agents as evidenced by enhanced fluorescence of the free reporter dye (Figure 1a). Measurements were performed at 37 °C and constant stirring. 100 × 10<sup>-6</sup> m LUVs were added to the pre-warmed buffer (50 × 10<sup>-3</sup> m NaCl, 10 × 10<sup>-3</sup> m HEPES, pH 7.5) and fluorescence was monitored for 100 s to obtain the baseline fluorescence value (set to 0%). Then NPs were added at different concentrations (Aerosil200: 25, 50, 67, 100 µg mL<sup>-1</sup>, colloidal SiO<sub>2</sub>-70 nm NPs: 25, 50, 100, 150, 200, 300 µg mL<sup>-1</sup> and SiO<sub>2</sub>-500 nm MPs: 60, 120, 240, 480, 960 µg mL<sup>-1</sup>, TiO<sub>2</sub> NPs: 100 µg mL<sup>-1</sup>) in a total volume of 1.5 mL and monitored for 15 to 30 min. Finally, the detergent Triton X-100 was added to a final concentration of 0.5% v/v to induce total LUV rupture (set to 100%). The fluorescence intensity of the reporter dye was a direct read-out for membranolysis upon permeabilization of

LUVs. Fluorescence was recorded on a spectrofluorimeter (FluoroMax2, HORIBA Yvon, Edison, NJ, US) with excitation wavelength set at 450 nm and emission wavelength at 530 nm.

**Vesicle binding assay:** In order to analyze membrane binding of silica particles, LUVs were prepared as described for the membranolysis assay.  $100 \times 10^{-6}$  M LUVs were added to the pre-warmed buffer ( $50 \times 10^{-3}$  M NaCl,  $10 \times 10^{-3}$  M HEPES, pH 7.5), followed by the addition of different concentrations of NPs (12.5, 25, 50, 100, 200, and  $300 \mu\text{g mL}^{-1}$ ) to a final volume of 1.5 mL. After 30 min incubation at  $37^\circ\text{C}$  in the dark, the suspension was centrifuged at  $18\,000 \times g$  at  $20^\circ\text{C}$  for 40 min. While NPs and NP bound membranes settle down, unruptured vesicles were located in the supernatant. Then, the supernatants were collected and  $100 \mu\text{L}$  in duplicates were transferred to a flat bottom 96-well plate. Fluorescence measurements were performed by using a fluorescence microplate reader (MWG Biotech AG, Ebersberg, Germany) at 560 nm excitation and 620 nm emission wavelength. Fluorescence intensities of the samples were normalized to untreated LUVs control values which were set to 100%.

**Cell culture, particle exposure, and LDH release assay:** The A549 cells were grown in DMEM supplemented with 10% FBS,  $2 \times 10^{-3}$  M L-glutamine,  $100 \mu\text{g mL}^{-1}$  penicillin, and  $100 \text{ U mL}^{-1}$  streptomycin and split every 3 to 4 days.

LDH in the supernatant medium was an indicator of plasma membrane rupture and thus for necrotic cell death. The assay had been performed as described previously<sup>[41]</sup> according to the manufacturer's instructions. Briefly, to determine the release of LDH in the medium supernatant, A549 cells were seeded with a cell density of  $3.3 \times 10^4 \text{ cm}^{-2}$  in a 24-well. On the next day, the medium supernatant was removed and fresh medium-containing particles were added to the cells, which were incubated with different concentrations of silica NPs (5, 10, 25, 50, 100, and  $200 \mu\text{g mL}^{-1}$ ) for 24 h. As positive control cells were completely lysed with 0.1% Triton X-100. To measure the optical density at 450 nm, the microplate reader VERSAmax and the software package SoftMaxPro (Molecular Devices, Ismaning, Germany) were applied and the relative amount of released LDH in the samples was normalized to the total amount of LDH of the Triton control.

**Molecular modeling:** MD simulations were performed for the interactions of lipids with the silica surface using the GROMACS simulation suite and the AMBER99SB-ILDN force field. Models for the silica surface were generated from the work by Emami et al.,<sup>[52]</sup> which provided a validated library of surface models for silica surfaces. These models provided the atomic coordinates for the surface atoms with various degrees of protonation depending on pH and were used as the input for the MD simulations. Dependent on synthesis, thermal treatment, and other factors, silica surface features could vary displaying, e.g., different amounts of geminal silanols (Q2), isolated silanols (Q3), and siloxane bridges (Q4). Here, a regular Q3 surface resembling the surface properties of hydrophilic, amorphous silica was used with 4.7 silanol groups  $\text{nm}^{-2}$ . The model surface allowed to simulate different ionization levels (0–18%) depending on the pH (2–9). Models for the lipids were generated based on standard structures available from the protein database (RCSB PDB, <http://www.rcsb.org>). The molecules were parameterized for the simulations with the force field specified above using AmberTools (<http://ambermd.org>) and ACPYPE, the simulations results were visualized using PyMol (PyMOL.org) and Open Babel (openbabel.org). To compute the binding energy profiles, umbrella sampling simulations were performed using 171 windows evenly spaced between 0.21 and 1.94 nm.<sup>[72]</sup> To analyze the interactions of the lipids with specific groups on the surface, unbiased MD simulations were performed for each surface model and computed histograms of the surface coverage by individual groups.

## Supporting Information

Supporting Information is available from the Wiley Online Library or from the author.

## Acknowledgements

The authors thank Dr. Johannes Reichert (IBG2, KIT) for his contribution in terms of experimental design, lipid vesicle preparation, and data analysis. A part of this work (R.L.) was supported by a grant from the Federal Institute for Risk Assessment (BfR), Germany (BfR-ZEBET-1329-475) which is greatly acknowledged.

Open access funding enabled and organized by Projekt DEAL.

## Conflict of Interest

The authors declare no conflict of interest.

## Author Contributions

R.L. and S.F.D. contributed equally to this work.<sup>[72]</sup> R.L., S.F.D., P.W., S.D., and C.W. conceived and designed the experiments. R.L. and S.F.D. performed the experiments. F.G. and W.W. performed molecular dynamics simulations. R.L., S.F.D., and C.W. analyzed the data. R.L., S.F.D., A.U., and C.W. wrote the paper. All authors discussed the results and commented on the manuscript.

## Data Availability Statement

The data that support the findings of this study are available from the corresponding author upon reasonable request.

## Keywords

biocompatibility, material phospholipid interactions, membranes, membranolysis, nanoparticles

Received: December 5, 2022

Revised: March 22, 2023

Published online:

- [1] T. Gebel, H. Foth, G. Damm, A. Freyberger, P. J. Kramer, W. Lilienblum, C. Röhl, T. Schupp, C. Weiss, K. M. Wollin, J. G. Hengstler, *Arch. Toxicol.* **2014**, *88*, 2191.
- [2] I. Lynch, C. Weiss, E. Valsami-Jones, *Nano Today* **2014**, *9*, 266.
- [3] C. Weiss, M. Carriere, L. Fusco, I. Capua, J. A. Regla-Nava, M. Pasquali, J. A. Scott, F. Vitale, M. A. Unal, C. Mattevi, D. Bedognetti, A. Merkoci, E. Tasciotti, A. Yilmazer, Y. Gogotsi, F. Stellacci, L. G. Delogu, *ACS Nano* **2020**, *14*, 6383.
- [4] D. Napierska, L. C. Thomassen, D. Lison, J. A. Martens, P. H. Hoet, *Part. Fibre Toxicol.* **2010**, *7*, 39.
- [5] M. W. Ambrogio, C. R. Thomas, Y. L. Zhao, J. I. Zink, J. F. Stoddart, *Acc. Chem. Res.* **2011**, *44*, 903.
- [6] A. M. Nyström, B. Fadeel, *J. Controlled Release* **2012**, *161*, 403.
- [7] J. G. Croissant, K. S. Butler, J. I. Zink, C. J. Brinker, *Nat. Rev. Mater.* **2020**, *5*, 886.
- [8] A. E. Nel, L. Mädler, D. Velegol, T. Xia, E. M. Hoek, P. Somasundaran, F. Klaessig, V. Castranova, M. Thompson, *Nat. Mater.* **2009**, *8*, 543.
- [9] M. Zhu, G. Nie, H. Meng, T. Xia, A. Nel, Y. Zhao, *Acc. Chem. Res.* **2013**, *46*, 622.
- [10] S. Halappanavar, S. van den Brule, P. Nymark, L. Gate, C. Seidel, S. Valentino, V. Zhernovkov, P. Høgh Danielsen, A. De Vizcaya,

- H. Wolff, T. Stoger, A. Boyadziev, S. S. Poulsen, J. B. Sorli, U. Vogel, *Part. Fibre Toxicol.* **2020**, *17*, 16.
- [11] P. Roach, D. Farrar, C. C. Perry, *J. Am. Chem. Soc.* **2006**, *128*, 3939.
- [12] Z. J. Deng, M. T. Liang, M. Monteiro, I. Toth, R. F. Minchin, *Nat. Nanotechnol.* **2011**, *6*, 39.
- [13] J. D. Harley, J. Margolis, *Nature* **1961**, *189*, 1010.
- [14] C. Pavan, M. Tomatis, M. Ghiazza, V. Rabolli, V. Bolis, D. Lison, B. Fubini, *Chem. Res. Toxicol.* **2013**, *26*, 1188.
- [15] H. Zhang, D. R. Dunphy, X. Jiang, H. Meng, B. Sun, D. Tarn, M. Xue, X. Wang, S. Lin, Z. Ji, R. Li, F. L. Garcia, J. Yang, M. L. Kirk, T. Xia, J. I. Zink, A. Nel, C. J. Brinker, *J. Am. Chem. Soc.* **2012**, *134*, 15790.
- [16] V. Rabolli, L. C. Thomassen, C. Princen, D. Napierska, L. Gonzalez, M. Kirsch-Volders, P. H. Hoet, F. Huaux, C. E. Kirschhock, J. A. Martens, D. Lison, *Nanotoxicology* **2010**, *4*, 307.
- [17] Y. S. Lin, C. L. Haynes, *J. Am. Chem. Soc.* **2010**, *132*, 4834.
- [18] A. Lesniak, F. Fenaroli, M. P. Monopoli, C. Aberg, K. A. Dawson, A. Salvati, *ACS Nano* **2012**, *6*, 5845.
- [19] A. Panas, C. Marquardt, O. Nalcaci, H. Bockhorn, W. Baumann, H. R. Paur, S. Mülhopt, S. Diabaté, C. Weiss, *Nanotoxicology* **2013**, *7*, 259.
- [20] S. Tenzer, D. Docter, J. Kuharev, A. Musyanovych, V. Fetz, R. Hecht, F. Schlenk, D. Fischer, K. Kiouptsi, C. Reinhardt, K. Landfester, H. Schild, M. Maskos, S. K. Knauer, R. H. Stauber, *Nat. Nanotechnol.* **2013**, *8*, 772.
- [21] R. Iler, in *Health Effects of Synthetic Silica Particulates STP386655* (Ed: D. Dunnom), ASTM International, West Conshohocken, PA **1981**, pp. 3–29.
- [22] T. Nash, A. C. Allison, J. S. Harington, *Nature* **1966**, *210*, 259.
- [23] A. Vakurov, R. Brydson, A. Nelson, *Langmuir* **2012**, *28*, 1246.
- [24] A. Vakurov, R. Drummond-Brydson, N. William, D. Sanver, N. Bastús, O. H. Moriones, V. Puentes, A. L. Nelson, *Langmuir* **2022**, *38*, 5372.
- [25] M. R. de Planque, S. Aghdaei, T. Roose, H. Morgan, *ACS Nano* **2011**, *5*, 3599.
- [26] K. A. Dawson, A. Salvati, I. Lynch, *Nat. Nanotechnol.* **2009**, *4*, 84.
- [27] A. M. Farnoud, S. Nazemidashtarjandi, *Environ. Sci.: Nano* **2019**, *6*, 13.
- [28] E. Rideau, R. Dimova, P. Schwille, F. R. Wurm, K. Landfester, *Chem. Soc. Rev.* **2018**, *47*, 8572.
- [29] A. Asghari Adib, S. Nazemidashtarjandi, A. Kelly, A. Kruse, K. Cimat, A. E. David, A. M. Farnoud, *Environ. Sci.: Nano* **2018**, *5*, 289.
- [30] A. Lesniak, A. Salvati, M. J. Santos-Martinez, M. W. Radomski, K. A. Dawson, C. Åberg, *J. Am. Chem. Soc.* **2013**, *135*, 1438.
- [31] A. R. Ferhan, G. J. Ma, J. A. Jackman, T. N. Sut, J. H. Park, N.-J. Cho, *Sensors* **2017**, *17*, 1484.
- [32] S. Mornet, O. Lambert, E. Duguet, A. Brisson, *Nano Lett.* **2005**, *5*, 281.
- [33] H. I. Alkhamash, N. Li, R. Berthier, M. R. R. de Planque, *Phys. Chem. Chem. Phys.* **2015**, *17*, 15547.
- [34] O. Le Bihan, P. Bonnafous, L. Marak, T. Bickel, S. Trépout, S. Mornet, F. De Haas, H. Talbot, J.-C. Taveau, O. Lambert, *J. Struct. Biol.* **2009**, *168*, 419.
- [35] A. Zhang, A. Nelson, P. Beales, *Langmuir* **2012**, *28*, 12831.
- [36] X. Wei, W. Jiang, J. Yu, L. Ding, J. Hu, G. Jiang, *J. Hazard. Mater.* **2015**, *287*, 217.
- [37] B. Wang, L. Zhang, S. C. Bae, S. Granick, *Proc. Natl. Acad. Sci. U. S. A.* **2008**, *105*, 18171.
- [38] K. Donaldson, P. J. Borm, G. Oberdörster, K. E. Pinkerton, V. Stone, C. L. Tran, *Inhalation Toxicol.* **2008**, *20*, 53.
- [39] S. Diabaté, L. Armand, S. Murugadoss, M. Dilger, S. Fritsch-Decker, C. Schlager, D. Béal, M.-E. Arnal, M. Biola-Clier, S. Ambrose, S. Mülhopt, H.-R. Paur, I. Lynch, E. Valsami-Jones, M. Carriere, C. Weiss, *Nanomaterials* **2021**, *11*, 65.
- [40] R. J. Mason, M. C. Williams, *Biochim. Biophys. Acta* **1980**, *617*, 36.
- [41] R. Leibe, I. L. Hsiao, S. Fritsch-Decker, U. Kielmeier, A. M. Wagbo, B. Voss, A. Schmidt, S. D. Hessman, A. Duschl, G. J. Oostingh, S. Diabaté, C. Weiss, *Arch. Toxicol.* **2019**, *93*, 871.
- [42] S. Murugadoss, D. Lison, L. Godderis, S. van den Brule, J. Mast, F. Brassinne, N. Sebaihi, P. H. Hoet, *Arch. Toxicol.* **2017**, *91*, 2967.
- [43] M. Crowe, Y. Lai, Y. Wang, J. Lu, M. Zhao, Z. Tian, J. Long, P. Zhang, J. Diao, *Small Methods* **2017**, *1*, 1700207.
- [44] H. Kettiger, G. Québatte, B. Perrone, J. Huwyler, *Biochim. Biophys. Acta, Biomembr.* **2016**, *1858*, 2163.
- [45] I. I. Slowing, C. W. Wu, J. L. Vivero-Escoto, V. S. Lin, *Small* **2009**, *5*, 57.
- [46] C. Pavan, M. J. Sydor, C. Bellomo, R. Leinardi, S. Cananà, R. L. Kendall, E. Rebba, M. Corno, P. Ugliengo, L. Mino, A. Holian, F. Turci, *Colloids Surf., B* **2022**, *217*, 112625.
- [47] F. C. Tsui, D. M. Ojcius, W. L. Hubbell, *Biophys. J.* **1986**, *49*, 459.
- [48] M. Delle Piane, S. Potthoff, C. Brinker, L. Ciacchi, *J. Phys. Chem. C* **2018**, *122*, 21330.
- [49] X. Wei, N. Liu, J. Song, C. Ren, X. Tang, W. Jiang, *Sci. Total Environ.* **2022**, *838*, 156552.
- [50] S. Yuan, H. Zhang, X. Wang, H. Zhang, Z. Zhang, S. Yuan, *Colloids Surf., B* **2022**, *210*, 112250.
- [51] C. Sögaard, J. Funehag, Z. Abbas, *Nano Convergence* **2018**, *5*, 6.
- [52] F. S. Emami, V. Puddu, R. J. Berry, V. Varshney, S. V. Patwardhan, C. C. Perry, H. Heinz, *Chem. Mater.* **2014**, *26*, 2647.
- [53] C. Pavan, R. Santalucia, R. Leinardi, M. Fabbiani, Y. Yakoub, F. Uwambayinema, P. Ugliengo, M. Tomatis, G. Martra, F. Turci, D. Lison, B. Fubini, *Proc. Natl. Acad. Sci. U. S. A.* **2020**, *117*, 27836.
- [54] T. N. Sut, A. R. Ferhan, S. Park, D. J. Koo, B. K. Yoon, J. A. Jackman, N.-J. Cho, *Appl. Mater. Today* **2022**, *29*, 101618.
- [55] F. Wang, J. Liu, *Small* **2014**, *10*, 3927.
- [56] X. Wang, X. Li, H. Wang, X. Zhang, L. Zhang, F. Wang, J. Liu, *Langmuir* **2019**, *35*, 1672.
- [57] F. Wang, J. Liu, *J. Am. Chem. Soc.* **2015**, *137*, 11736.
- [58] H. Ruh, B. Kühl, G. Brenner-Weiss, C. Hopf, S. Diabaté, C. Weiss, *Toxicol. Lett.* **2012**, *208*, 41.
- [59] Y. Hayashi, T. Miclaus, S. Murugadoss, M. Takamiya, C. Scavenius, K. Kjaer-Sorensen, J. J. Enghild, U. Strähle, C. Oxvig, C. Weiss, D. S. Sutherland, *Environ. Sci.: Nano* **2017**, *4*, 895.
- [60] I. L. Hsiao, S. Fritsch-Decker, A. Leidner, M. Al-Rawi, V. Hug, S. Diabaté, S. L. Grage, M. Meffert, T. Stoeger, D. Gerthsen, A. S. Ulrich, C. M. Niemeyer, C. Weiss, *Small* **2019**, *15*, 1805400.
- [61] M. Wiemann, A. Vennemann, U. G. Sauer, K. Wiench, L. Ma-Hock, R. Landsiedel, *J. Nanobiotechnol.* **2016**, *14*, 16.
- [62] M. Arribas Perez, P. A. Beales, *Langmuir* **2021**, *37*, 13917.
- [63] E. Melby, A. Mensch, S. Lohse, D. Hu, G. Orr, C. Murphy, R. Hamers, J. Pedersen, *Environ. Sci.: Nano* **2015**, *3*, 45.
- [64] G. van Meer, D. R. Voelker, G. W. Feigenson, *Nat. Rev. Mol. Cell Biol.* **2008**, *9*, 1102.
- [65] I. D. Pogozheva, G. A. Armstrong, L. Kong, T. J. Hartnagel, C. A. Carpino, S. E. Gee, D. M. Picarello, A. S. Rubin, J. Lee, S. Park, A. L. Lomize, W. Im, *J. Chem. Inf. Model.* **2022**, *62*, 1036.
- [66] S. P. Mukherjee, B. Lazzaretto, K. Hultenby, L. Newman, A. F. Rodrigues, N. Lozano, K. Kostarelos, P. Malmberg, B. Fadeel, *Chem* **2018**, *4*, 334.
- [67] K. Rasmussen, J. Mast, P. J. De Temmerman, E. Verleysen, N. Waegeneers, F. Van Steen, J. C. Pizzolon, L. De Temmerman, E. Van Doren, K. A. Jensen, R. Birkedal, M. Levin, S. H. Nielsen, I. K. Koponen, P. A. Clausen, V. Kofoed-Sorensen, Y. Kembouche, N. Thieriet, O. Spalla, C. Guiot, D. Rousset, O. Witschger, S. Bau, B. Bianchi, C. Motzkus, B. Shvachev, L. Dimova, R. Nikolova, D. Nihtianova, M. Tarassov, et al., *Titanium dioxide, NM-100, NM-101, NM-102, NM-103, NM-104, NM-105: Characterisation and Physico-chemical Properties*, Publications Office of the European Union, Luxembourg **2014**.
- [68] S. Mülhopt, S. Diabaté, M. Dilger, C. Adelhelm, C. Anderlohr, T. Bergfeldt, d. I. T. Gomez, Y. Jiang, E. Valsami-Jones, D. Langevin,

- I. Lynch, E. Mahon, I. Nelissen, J. Piella, V. Puentes, S. Ray, R. Schneider, T. Wilkins, C. Weiss, H. R. Paur, *Nanomaterials* **2018**, *8*, 311.
- [69] D. J. Giard, S. A. Aaronson, G. J. Todaro, P. Arnstein, J. H. Kersey, H. Dosik, W. P. Parks, *J. Natl. Cancer Inst.* **1973**, *51*, 1417.
- [70] M. Lieber, B. Smith, A. Szakal, W. Nelson-Rees, G. Todaro, *Int. J. Cancer* **1976**, *17*, 62.
- [71] P. Wadhvani, J. Reichert, J. Burck, A. S. Ulrich, *Eur. Biophys. J.* **2012**, *41*, 177.
- [72] J. Kästner, *Wiley Interdiscip. Rev.: Comput. Mol. Sci.* **2011**, *1*, 932.